POLITECNICO DI TORINO

**Corso di Laurea Magistrale
in Ingegneria Aerospaziale**

Tesi di Laurea Magistrale

Analysis and implementation of the actuator line method for aeronautical propellers

1859

Relatori
prof. Andrea Ferrero
prof. Francesco Larocca
prof. Dario Pastrone

Candidato
Lorenzo Pagella

Anno Accademico 2021-2022

Summary

The analysis of propellers is characterized by a great variety of available methods to evaluate their performance, with different levels of accuracy and computational cost. Some widely used analytical methods are based on a series of approximations which allow to perform calculations, in a reduced amount of time and with an acceptable level of accuracy. Among them, the Momentum theory and Blade Element Theory (BET) should be cited, as well as the Blade Element Momentum Theory (BEMT) which is a combination of the previous two. The introduction of computational fluid-dynamics techniques based on the resolution of Navier-Stokes equations has brought to the development of simulations with a high accuracy but, usually, a very high computational cost. In the last decades researcher's efforts have been spent in the evaluation of the possibility to develop new methods which can somehow combine the computational efficiency of the Blade Element Momentum Theory and the accuracy guaranteed by CFD techniques. This context has brought to the introduction of the Actuator Disk Method (ADM) and then of the more accurate Actuator Line Method (ALM). These techniques have followed the idea of approximating the propeller as a source of momentum which is then introduced in the resolution of the Navier-Stokes equations. In the actuator disk method, forces exchanged between propeller and fluid are seen as evenly distributed on a zero-thickness disk, while in the actuator line method these forces are radially distributed along lines which represent propeller's blades. The goal of this thesis is the implementation of the Actuator Line Method in a CFD code and its application to the analysis of a propeller for which geometry and experimental data are known, comparing propeller's performance resulting from the implemented model with propeller's performance given by experiments in wind tunnels and other numerical data available in the literature.

In the first chapter a brief introduction will be presented, in which the central topics will be the evaluation of the advantages and the disadvantages of the different available methods and the needs that have brought to the introduction of the Actuator Line Method. In the second chapter the methods today available for the analysis of an aeronautical propeller will be presented, in particular: Momentum Theory, Blade Element Theory and Blade Element Momentum Theory; methods that implement a full resolution of the flow acting on a propeller through high fidelity computational fluid-dynamics simulations; the Actuator Disk Method. In the third chapter a detailed explanation of the Actuator Line Method will be performed, focusing in particular on the strategies adopted during the implementation of the code. The fourth chapter will provide all the details regarding the case study considered, relevant data about propeller's geometry will be reported and also the results of experimental analysis. In the fifth chapter results obtained through the implementation of the Actuator Line Method will be shown, evaluating the accuracy of the method and the computational cost required by the simulations.

Acknowledgements

I'm very grateful to my mother for having supported me and encouraged me to do my best, accompanying me along all these years. I'm also thankful to my father for his support and for all the precious advice he gave to me.

I'm very grateful to my grandmothers for all the unconditional love they have gifted me with along these years, as they always have.

I'm thankful to my sister Cecilia and my brother Leonardo, for being always by my side and for being the ones I can always rely on. I would also like to thank my aunt, my uncle and Matteo, for being always ready to help me and to give me advice.

I'm grateful to all my closest friends, for having supported me and especially for having made me smile, even in the less simple moments of this journey.

I'm very grateful to Professor Andrea Ferrero, for having patiently given me suggestions and guided me during the drafting of this thesis, and for all the time he has devoted to help me.

Contents

List of Tables

List of Figures

Part I

Methods for propeller analysis and implementation of the ALM

Chapter 1

Introduction

The analysis of propellers has always been a topic of great interest in aeronautics. Today, this device has gained even more relevance because of the development of new architectures such as aerotaxis, distributed propulsion electrical aircrafts equipped with a large number of propellers, or even unmanned aerial vehicles (UAVs) and micro air vehicles (MAVs).

Most of the available analytical techniques for analyzing the performance of an aeronautical propeller are today based on the Blade-Element Momentum Theory (BEMT) (Glauert [1926]), which combines the Blade Element Theory (BET) (Drzewiecki [1920]) with the Momentum Theory (Rankine [1865], Froude [1889]). Momentum Theory, assumes forces exchanged between flow and propeller as evenly distributed on a zero thickness disk. Various assumptions are made: the flow considered is inviscid, incompressible and steady; velocity and static pressure are seen as uniform over each cross section of the disk. This is a very simple method but with quite low reliability. BEMT is based on the subdivision of the flow in annular control volumes, and on the application of the conservation laws in each control volume. The annular volumes are bounded by stream surfaces that extend from far upstream to far downstream. The aerodynamic forces acting on the blade element considered are deduced through the use of tabulated airfoil data, which are derived from experimental measurements carried on in wind tunnels. There is the need to introduce a series of assumptions: the flow has to be axis-symmetric, the flow can be studied through the subdivision in radially separated streamtubes. Moreover, because of these assumptions, it is necessary to introduce a certain number of empirical corrections; owing to limitations of representing, for example, phenomena related to: dynamic inflow, yaw misalignment, tip loss and heavily loaded rotors. Methods based on the BEMT have been vastly used for the analysis of many devices, such as propellers (Tognaccini [2014]), helicopter rotors or wind turbines; they are simple, fast and quite reliable. All the analytical techniques available for the evaluation of aeronautical propellers' performance are categorized as low fidelity methods.

The most reliable methods for the analysis of an aircraft propeller are fully resolved, three-dimensional, CFD simulations. These types of analysis allow to predict with high accuracy the behaviour of a propeller in different working conditions, thanks to a complete resolution of the Navier-Stokes equations. Computational fluid-dynamics simulations are

categorized as high fidelity methods. In the bibliography, comparisons between the computationally cheap BEMT and the highly accurate CFD simulations for the performance of an aircraft propeller can be found in Loureiro et al. [2021] or Carroll [2013]. However, the computational cost required is noticeably high and this has lead to the introduction of advanced techniques, which can provide a good reliability, while reducing the computational cost.

Among these methods one of the most relevant is the Actuator Disk Method (ADM), which is presented in Sørensen and Myken [1992]; it employs tabulated airfoil data along with the conservation laws. This method, with respect to the BEMT, eliminates the assumption of flow travelling in radially independent streamtubes, and introduce instead a numerical resolution of a full set of Navier-Stokes equations where source of momentum terms are introduced following the Momentum Theory. Forces are assumed to be evenly distributed on a zero-thickness permeable disk. However, the assumption of axis-symmetric flow is still valid also for the Actuator Disk Method. This is one of the most diffused between the nowadays existing techniques.

In order to overcome the limits imposed by the axis-symmetric flow approximation, Sorensen and Shen [2002] have introduced the Actuator Line Method (ALM), which combines a Navier-Stokes solver with a technique that assumes the acting forces as radially distributed over lines which represent the propeller's blades. The fluid mechanics governing equations are the Navier-Stokes equations for incompressible flows and the aerodynamic forces acting on each actuator line are introduced into the fluid-dynamics equations, which are solved by means of CFD techniques. This method was at first implemented, and later validated, in order to solve fluxes on wind turbines, and it has provided highly reliable results if compared to other currently available methods, or to experimental data. Moreover, the computational cost is relatively reduced and the required mesh is significantly simpler. It has also been verified that there are small differences in the wake structure between fully resolved CFD and ALM simulations, while using turbulent inflow. For all these reasons, the Actuator Line Method is found very attractive, if compared to other available types of simulations.

The goal of this thesis is to apply this method to solve fluxes acting on propellers used in aeronautical field, and verify its reliability through the analysis of a relevant case study. The propeller analyzed is the one designed by Weick and described in bibliography (Weick [1930]). Comparisons were made between results obtained with the actuator line method and experimental data, which have proven the adopted resolution method as reliable. Propeller's performance obtained with ALM have also been compared to the ones found by means of a method based on the BEMT, implemented by Tognaccini [2014]. Moreover, different grids have been adopted in order to evaluate the influence of domain size and mesh resolution.

Chapter 2

The analysis of an aeronautical propeller

The analysis of a propeller is characterized by many difficulties because a complete analysis of the flow field should consider a viscous, unsteady and compressible flow around complex geometries. An aeronautical propeller is used to accelerate air particles, while obtaining a propulsive force acting on itself, the thrust T. A propeller can be defined by three fundamental geometric entities: the diameter D, the local chord length c, and the local pitch angle γ; with c and γ that change with the radial position. Considering a flow with asymptotic velocity V_∞, the operating regime of a propeller is given by the advance ratio:

$$J = \frac{V_\infty}{nD};\tag{2.1}$$

where n is the rotational frequency of the propeller, expressed in $[round/s]$. Thrust and required power can be easily studied while introducing the dimensionless coefficients:

$$C_T = \frac{T}{\rho n^2 D^4};\tag{2.2}$$

$$C_P = \frac{P}{\rho n^3 D^5}.\tag{2.3}$$

These coefficients are linked by the definition of another dimensionless variable, the efficiency:

$$\eta = \frac{JC_T}{C_P}.\tag{2.4}$$

The curves reporting C_T, C_P and η given as functions of the advance ratio are the characteristic curves of a propeller. In the following chapters we will report a brief description of the most diffused methods for propeller analysis: fully resolved three-dimensional CFD simulations, the Blade Element Momentum Theory (BEMT), the Actuator Disk Method (ADM) and the Actuator Line Method (ALM).

2.1 The Momentum Theory

In order to overcome some of the difficulties in the propeller's analysis, approximations can be adopted while giving up the detailed knowledge of the flow-field in the proximity of the propeller. The Momentum theory has been introduced by Rankine [1865] and later continued by Froude [1889]; it considers the propeller as a zero-thickness disk which is modelled as a discontinuity surface for the flow field and thrust is uniformly distributed over the disk. There are some simplifying assumptions: the flow is considered inviscid, incompressible and steady; velocity and static pressure are assumed to be uniform over each cross section of the disk; pressure far ahead and far behind the disk matches the ambient value. In this approximation, the first half of the acceleration happens in front of the propeller, and the second half takes place behind the propeller. We know that the mass flow should be continuous, while discontinuities in pressure are admitted. Moreover, the energy level of the flow downstream of the disk is different from that of the external flow and this leads to the development of the propeller's wake. Energy variation imparted to the flow passing through the propeller has to be equal, due to energy conservation, to the expended energy provided to the propeller by the engine.

As reported by Tognaccini [2014] and by Rwigema [2010], the thrust produced by a propeller must be equal to the change in flow momentum along a stream-tube, following the axial direction. In the Actuator Disk model, the disk is seen as a discontinuity surface and pressure rises discontinuously through it from a value p^- immediately upstream to a value p^+ immediately downstream. The momentum balance is applied to the volume included between surfaces S_∞ and A, where A is the actuator disk section and S_∞ is the surface that delimits the stream-tube which goes from far upstream to far downstream. The velocity component normal to the disk is continuous through the disk, so that the momentum flow depends only on the pressure component and the thrust produced can be written as:

$$T = \Delta p A = \vec{k} * \int_{S_\infty} (pI + \rho \vec{V}\vec{V}) * \vec{n} \quad dS. \tag{2.5}$$

Where $\vec{n}$ is the versor normal to surface S_∞, $\vec{k}$ is the versor in axial direction and I is the identity matrix. Considering the inlet section of the stream-tube as section 0, and the outlet section as section e, we can write the conservation of mass along the stream-tube passing through the disk:

$$A_0 V_0 = AV = A_e V_e; \tag{2.6}$$

where V is the absolute velocity at the actuator disk section and A is the corresponding area.

Combining the previous equations and decomposing $S\infty$ in lateral surface S_t, inlet section A_0, and outlet section A_e, we can write a different formulation for the thrust generated by the propeller:

$$T = \dot{m}(V_e - V_0) + (p_e - p_0)A_e + \vec{k} * \int_{S_t} (p - p_0) * \vec{n} \quad dS. \tag{2.7}$$

A simple representation of the surfaces considered is reported in figure 2.1.
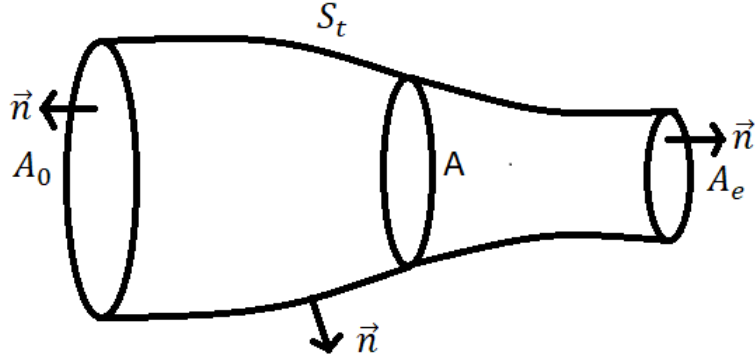
Figure 2.1.   Surfaces delimiting the stream-tube.

We can consider the lateral surface of the stream-tube as a surface through which the momentum flow is equal to zero and account only for the mass conservation through the surfaces far ahead and far behind the disk. Under these considerations, the last term of equation (2.7) will be equal to zero, and the thrust equation will become:

$$T = \dot{m}(V_e - V_0) + (p_e - p_0)A_e. \tag{2.8}$$

As written before, the first version of the Momentum Theory has been developed by Rankine [1865] in the second half of nineteenth century and it is usually referred to as "simple" momentum theory. Some other hypothesis are introduced: all the physical variables depends only on the axial position in the stream-tube, there are no discontinuities in the tangential velocity component through the disk (the disk does not introduce any rotational component in the flow, this is a strong approximation); this last hypothesis allows us to consider $p_e = p_0$ and equation (2.8) becomes:

$$T = \dot{m}(V_e - V_0). \tag{2.9}$$

Which can be also written as:

$$T = \rho V A(V_e - V_0). \tag{2.10}$$

It is also possible to write the thrust produced by the propeller as:

$$T = (p^+ - p^-)A. \tag{2.11}$$

Applying Bernoulli's equation, which states that the total pressure is constant along any stream line, excluding lines passing through the disk; and remembering the assumption for which pressure far ahead and far behind the disk matches the ambient value, the following equation can be considered:

$$p^+ - p^- = \frac{1}{2}\rho(V_e^2 - V_0^2). \tag{2.12}$$

Combining the above equations shows that the absolute velocity at the actuator disk corresponds to the average of the velocities far upstream and far downstream:

$$V = \frac{V_0 + V_e}{2}. \tag{2.13}$$

This is in accordance with the assumption that the first half of the acceleration given by the propeller is produced in front of the propeller, while the second half takes place behind it. Indeed, if we write the jump in velocity along the stream-tube as $\Delta V = V_e - V_0$ and we consider this equation along with the equation (2.13), we can easily obtain:

$$V = \frac{\Delta V}{2} + V_0. \tag{2.14}$$

This means that the additional velocity far downstream is the exact double of the velocity addition at the actuator disk section.

While introducing the "induced velocity" as $V' = \frac{\Delta V}{2}$ and thanks to a recombination of the above equations, an interesting different formulation of the thrust produced by a propeller can be obtained:

$$T = 2\rho A V'(V_0 + V'). \tag{2.15}$$

This clearly states that the thrust grows if the propeller diameter is increased, and also that thrust increases if the induced velocity, and so the velocity addition between far ahead and far behind the propeller, is increased. Moreover, if we consider a propulsive propeller ($T > 0$), velocity increases along the stream-tube, and the stream-tube contracts along axial direction. These type of information are in agreement with the results given by other theories and confirmed by experimental data.

The power P expended in order to obtain the thrust T is given by the variation in kinetic energy experienced by the flow:

$$P = \frac{1}{2}\dot{m}(V_e^2 - V_0^2) = \frac{1}{2}T(V_e + V_0) = TV. \tag{2.16}$$

Thus, propeller's efficiency can be defined as:

$$\eta = \frac{TV_0}{P} = \frac{1}{1+a}. \tag{2.17}$$

Where $a = \frac{V'}{V_0}$ and is called the axial interference factor. From this last equation we can understand that, in order to obtain maximum efficiency from the propeller, given the thrust produced, it is necessary to minimize the axial interference factor, which means that the largest possible propeller's diameter should be adopted.
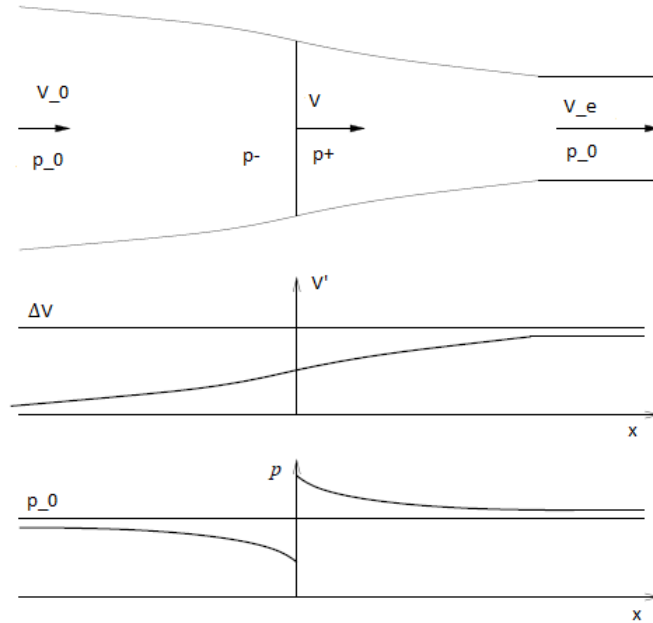
Figure 2.2. Actuator disk model in simple momentum theory (Tognaccini [2014]).

If the hypothesis of uniform axial induction on the propeller is removed then the axial interference factor must be considered variable along the radius; it is interesting to evaluate for which radial distribution of a the maximum efficiency is obtained. Another hypothesis has to be made: for each elementary annular surface of area $2\pi r dr$ there is no interaction with any other elementary surface. Therefore thrust can be calculated applying the results of simple momentum theory to the elementary annular surface. The so called differential simple momentum theory is obtained. This theory has shown that, if the thrust produced is known and the diameter of the propeller is fixed, then the maximum efficiency is obtained if the load is evenly distributed on the disk. Experimental evidences have demonstrated that quite accurate results can be obtained with this theory for propellers which are slightly loaded and have little rotational effects; however, the hypothesis of no interaction between different annular surfaces does not show a good agreement with the physics.

The simple momentum theory has been derived considering only axial velocity variations, while changes in radial and tangential velocities have been neglected. Propeller's rotation with a certain angular velocity obviously introduces a rotational velocity component downstream of the propeller. That's why Betz [1920] developed the so called "general" momentum theory, which accounts for the rotational velocity introduced. In this theory the effect of the radial velocity component is still neglected, as well as viscous losses due to the interaction between the propeller's blades and the flow. For these reasons, the ideal efficiency calculated by means of this theory can not be exceeded by

a real propeller. The general momentum theory gives us, for each value of J and C_T, the maximum level of efficiency that can not be overcome, whatever the geometry of the propeller is (Tognaccini [2014]).

2.2 The Blade Element Momentum Theory (BEMT)

2.2.1 Propeller's vortical system.

The generation of thrust by a propeller can be attributed to the lift acting on propeller's blades, and each blade can be considered as a finite wing which interacts with a flow of variable velocity; indeed, the rotational velocity, which depends on the radial position, has to be summed to the translational velocity of the propeller. Tognaccini [2014] reports that it is possible to develop a model in which the propeller is seen as a disk on which infinite vortices with intensity $\gamma(r)$ are radially distributed. The circulation at a certain radial position is given by:

$$\Gamma(r) = 2\pi\gamma(r)r. \tag{2.18}$$

The shape of vortices is helicoidal because they have to follow the trajectory of flow particles. If a slightly loaded propeller is considered, the effect of radial velocities can be neglected, under these assumptions, the propeller's wake is a cylinder which has for basis the actuator disk and is developed until far downstream. The helicoid described by each free vortex has a pitch (or aerodynamic pitch) p_a, which is the distance in axial direction between two different points of the helicoid and can be calculated as:

$$p_a = JD. \tag{2.19}$$

To fully understand the flow field generated by free vortices, we can consider it as equivalent to the field induced by the composition of a system of free straight vortices parallel to the axial direction, with a second system of concentric annular vortices which develops along the wake. Annular vortex system induces an axial velocity component inside the wake, at the propeller's section induction is due only to the annular vortex system which develops beginning from this section, while far downstream the contribution from the annular vortices developed far upstream should be added. The axial velocity component at a section positioned far downstream is found to be the double of the one acting on the propeller's disk, this conclusion is in agreement with the simple momentum theory. Rotational velocity outside the wake is equal to zero, indeed, if the circulation along a line downstream from the disk and enclosing all the wake is calculated, it results equal to zero. It can also be observed, with similar considerations, that the rotational velocity induced far downstream is two times the one induced on the disk. If the circulation around a single blade is Γ_b and the propeller has a certain number of blades N, the total circulation $\Gamma = \Gamma_b N$ can be related to the induced rotational velocity. Indeed, while summing the circulation on each blade, we obtain:

$$\Gamma = 2\pi r\omega. \tag{2.20}$$

Where ω is the induced rotational velocity. If we consider the wake of a propeller which is evenly loaded along the radius, free helicoidal vortices develop from the tip of

the blades with intensity: $\gamma = \frac{\Gamma}{2\pi R}$; with R radius of the disk. From the centre of the disk starts another straight vortex in axial direction, with intensity Γ.

2.2.2 The Blade Element Theory (BET)

We have to introduce now the so called Blade Element Theory (BET) which, merged to the previously described Momentum Theory, has brought to the Blade Element Momentum Theory (BEMT), a largely diffused method for the analysis of propellers. The idea of the blade element was first introduced by Drzewiecki [1920] to enhance the results produced by Froude [1889]. This theory allows the calculation of the differential thrust and torque at a given radial location on the propeller. The propeller, indeed, is divided into a number of sections and each of them is solved and then summed to the others in order to give the overall thrust and torque. This method uses a series of annular stream tubes control volumes, and each one of these volumes contains a distinct element of the blade, which has height dr. Geometrical properties, such as airfoil shape and chord or twist distribution are used to calculate the forces exchanged between the propeller and the flow-field. Two important assumptions are essentially made: there is supposed to be no interaction between fluxes acting on different blade element of the propeller; and the forces exerted by the flow on the propeller depends only on the two-dimensional lift and drag acting on each blade element. Since C_L and C_D are determined by knowing local Reynolds number and angle of attack, it is necessary to determine the flow angle ϕ, which is based on the two components of the local velocity vector, and is later used to calculate the local angle of attack α. At this point thrust and torque of the element are determined as:

$$\Delta T = \frac{1}{2}\rho V^2(C_L\cos\phi - C_D\sin\phi)cdr; \tag{2.21}$$

$$\Delta Q = \frac{1}{2}\rho V^2(C_L\sin\phi + C_D\cos\phi)crdr. \tag{2.22}$$

Where ρ and V are the flow density and velocity at the propeller plane. Finally the thrust and torque are summed over all elements of each blade and produced T and Q are calculated.

The description of the wake as a vortical system and the analogy with lifting line theory allows to overcome the contradictions between the blade element theory and the momentum theories. Blade Element Momentum Theory (BEMT), which was first proposed by Glauert [1926], combines BET and Momentum Theory and provides a way to evaluate the flow-field around a propeller. It also allows to alleviate the difficulties in calculating the induced velocities at the propeller, and to correct the inflow conditions assumed in the blade element theory. As in the case of the BET, the analysis is based on the differential thrust and torque of the propeller, which is modelled as an actuator disk. The propeller is divided again in a certain number of elements along the radius of each blade, and for each element a force balance is applied, considering two-dimensional lift and drag to calculate thrust and torque generated by the single section. This generates a set of nonlinear equations which can be solved iterating for each blade section, generally the quantity iterated is the thrust coefficient; then the overall thrust and torque can be

calculated. A brief description of the calculation generally adopted to calculate thrust and torque by means of the BEMT is reported here.

If the propeller's geometry, the number of blades and blades' geometry are known, the flow angle ϕ can be obtained as:

$$\tan \phi = \frac{V_0(1+a)}{\Omega r(1-a')}. \tag{2.23}$$

Where Ω is the angular velocity of the propeller and a' is the rotational interference factor, calculated as $a' = \frac{\omega}{2\Omega}$; with ω the induced angular velocity. The angle of attack is given by the difference between the pitch angle and the flow angle:

$$\alpha = \gamma - \phi. \tag{2.24}$$

The effective velocity is calculated as:

$$V_e = V_0^2(1+a)^2 + \Omega^2 r^2 (1-a')^2. \tag{2.25}$$
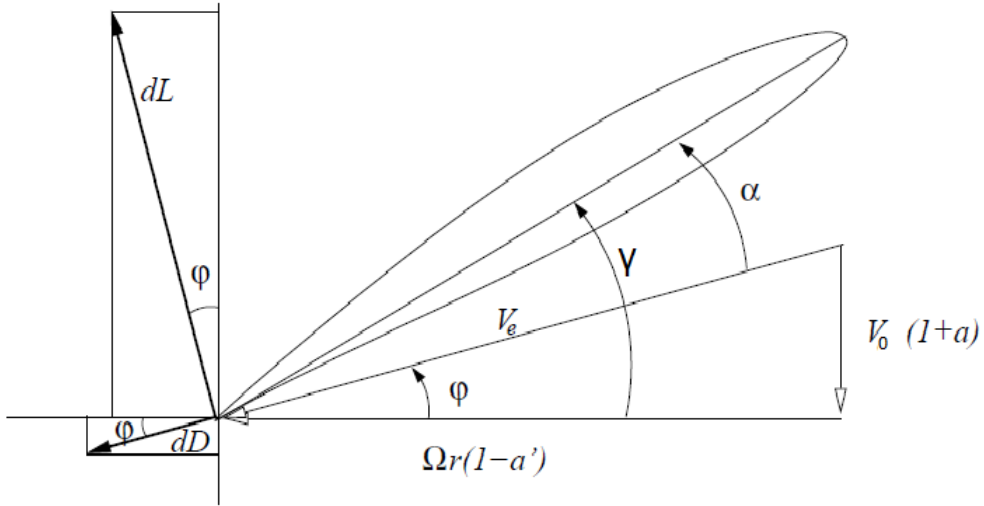
Figure 2.3. Effective velocity and flow angle in blade element theory (Tognaccini [2014]).

Then the thrust and torque acting on the single blade element are calculated with formulas 2.21 and 2.22, respectively, while using the effective velocity V_e instead of V. If N is the number of blades of the propeller and the solidity at radius r, $\sigma = \frac{Nc}{2\pi r}$, is introduced, thrust and torque for the entire propeller are:

$$\frac{dT}{dr} = \sigma \pi \rho r V_e^2 (C_L \cos \phi - C_D \sin \phi); \tag{2.26}$$

$$\frac{dQ}{dr} = \sigma \pi \rho r^2 V_e^2 (C_L \sin \phi + C_D \cos \phi).$$ (2.27)

It can be useful to observe that C_L and C_D are functions of the angle of attack α and of the local Reynolds number, but, for little values of α, dependence from Reynolds number can be neglected, therefor lift and drag coefficients can be calculated as functions of α. Relations obtained allows to evaluate the performances of a known propeller. If a non-viscous flow is considered, results derived from BEMT coincides with the ones obtained with general momentum theory. For the highest values of J, viscous effects cause a quite important difference between curves $\eta(J)$ obtained applying the two theories. When the pitch angle of the blade increases, the point of maximum efficiency shifts to the right because, at a certain rotational velocity, blade elements work at a lower α, and thus at a lower C_D, for higher values of V_0. This leads to an interesting consideration: a propeller can keep an high level of efficiency for a longer interval if the pitch angle γ changes for different values of advance ratio J; thus a variable pitch propeller should be adopted. Further studies about optimal working conditions for a propeller have brought to a relevant observation: a propeller with a certain thrust level reaches the maximum efficiency if the vortical wake shifts and rotates rigidly, generating an helicoidal surface with constant pitch (Tognaccini [2014]). The Blade Element momentum theory requires a low computational cost if compared to detailed CFD models, the accuracy of the results is obviously lower, but this technique can be adopted in the early stages of a propeller design.

2.3 High fidelity CFD simulations

As said before, the efficiency of the Blade Element Momentum Theory comes with a significant loss in accuracy with respect to full CFD resolution methods. For example, BEMT fails in predicting important 3D flow effects, such as tip losses, which can affect propeller performances. Tip losses happen when tip vortices are introduced in the propeller wake, causing a reduction of the thrust produced in the tip region of each blade. Post stall behaviour of a propeller is also bounded to 3D flow effects, propeller's rotation induce centrifugal and Coriolis forces on the blade and on the fluid particles around the blade surface. These forces produce a strong radial force component in the boundary layer and help stabilize it, this leads to a postponed separation for higher angles of attack on a 3D rotating propeller blade, if compared to a non-rotating one; with a positive effect on propeller's thrust. This effect is known as stall-delay and is stronger near the root and weaker in the tip region. Using high fidelity CFD it is possible to have a time-accurate simulation, where complicated 3D flow effects are taken into account and highly accurate results are obtained. Of course, a high resolution mesh is required, which has to adapt to the rotating blades; indeed, propeller CFD simulations often adopt a mesh around the propeller, or the single blade, which rotates relatively to a second stationary mesh. In addition, a time-dependent simulation has to work with very small time steps in order to resolve the fast propeller rotation, and it has to include several revolutions to obtain a periodic solution. These characteristics lead to a considerable time expense for a full CFD

simulation. This type of simulation is usually adopted when a very detailed flow analysis is required, and they are typically used in studies where few simulations are needed, but with the highest possible level of accuracy.

2.3.1   Steady state and unsteady approaches

There are many different full CFD methods to model rotating flows or to analyze propulsion systems' fluid-dynamics in general, and there are a lot of thesis or reviews which provide a general overview about this topic, for example, in the studies made by D'Ambrosio and Ruiz [2019]. CFD techniques often needs to consider a multiple reference frame, in which one reference frame is stationary while the other, which contains the propeller, has to rotate with a precise angular velocity. The various available methods which account for the propeller's rotation can be divided in two categories of approaches: steady state and unsteady state approaches.

Steady state approaches can be used to solve constant rigid body motion, but it has to be noted that the flow is still unsteady. A moving frame of reference should be used to describe rotating blades and time averaged characteristics of the flow should be computed. Moreover, free-stream velocity needs to be parallel to the axis of rotation and the volume containing the rotating region must be axisymmetric. These approaches can only be used when average values are relevant and transient effects can be neglected. It has to be observed that in this type of approaches the mesh does not move, the reference frame is rotating and the velocity components of the fluxes are calculated relatively to this moving reference frame, but the meshes are always static. Since we are considering stationary approaches, it is obvious that the Navier-Stokes equations will be used in their steady state form. Steady state Navier-Stokes equations in differential form and in absence of volume forces are:

$$\nabla * (\rho \vec{V}) = 0; \tag{2.28}$$

$$\nabla * (\rho \vec{V} \vec{V}) = -\nabla(p) + \nabla * (\tau). \tag{2.29}$$

Compressible Navier-Stokes equations are adopted in order to describe compressible flows in the presence of diffusive effects. If viscous effects are neglected, Euler equations are obtained, which are used to describe compressible flows in the absence of diffusive effects. These equations can be adopted to describe expansion and compression fans, shock waves and contact surfaces. Steady state Euler equations in differential form are:

$$\nabla * (\rho \vec{V}) = 0; \tag{2.30}$$

$$\nabla * (\rho \vec{V} \vec{V}) = -\nabla(p). \tag{2.31}$$

We can rewrite the absolute velocity in terms of relative velocities:

$$\vec{V} = \vec{v_r} + \vec{v_t} + (\vec{\omega} \times \vec{r}). \tag{2.32}$$

Then we can rewrite Navier-Stokes equations in the rotating frame of reference and express them in terms of relative velocity, combining the above equations:

$$\nabla * (\rho \vec{v_r}) = 0; \tag{2.33}$$

$$\nabla * (\rho \vec{v_r} \vec{v_r}) = -\nabla(p) + \mu \nabla * \nabla(\vec{v_r}) - \rho(2\vec{\omega} \times \vec{v_r}) - \vec{\omega} \times \vec{\omega} \times \vec{r}. \tag{2.34}$$

The last two terms in equation (2.34) are Coriolis and Centripetal accelerations, which are caused by the non-inertial reference frame considered.

Unsteady approaches consider moving meshes and have a very high computational cost but they are the only way of conducting simulations in order to obtain time accurate results. In this case unsteady Navier-Stokes equations in differential form are adopted. We can write, again neglecting volume forces:

$$\frac{\partial \rho}{\partial t} + \nabla * (\rho \vec{V}) = 0; \tag{2.35}$$

$$\frac{\partial \rho \vec{V}}{\partial t} + \nabla * (\rho \vec{V} \vec{V}) = -\nabla(p) + \nabla * (\tau). \tag{2.36}$$

For the sake of completeness, we report also unsteady Euler equations in differential form:

$$\frac{\partial \rho}{\partial t} + \nabla * (\rho \vec{V}) = 0; \tag{2.37}$$

$$\frac{\partial \rho \vec{V}}{\partial t} + \nabla * (\rho \vec{V} \vec{V}) = -\nabla(p). \tag{2.38}$$

In unsteady approaches usually the whole mesh rotates following an imposed motion that makes it follow the propeller, Navier-Stokes equations are thus solved for the moving mesh. Thanks to these methods we can observe also unsteady phenomena and we can have a better understanding of the propeller behavior and its performance; however the computational cost is even worse than in the steady state conditions. Along with these methods, techniques which combine rotating and static regions also exists; they are particularly useful if non axisymmetric domains are considered. We will have a rotating mesh in the regions occupied by propeller blades which slides along the boundaries of the steady control volume. These approaches necessitates to enable simulations across disconnected, but adjacent, mesh domains.

2.3.2 Turbulence models

Turbulent wakes are often present in simulations involving aeronautical propellers, and the behaviour of turbulence could be predicted adopting Direct Numerical Simulations (DNS), which integrates the three-dimensional Navier-Stokes equations. However, an accurate analysis of the turbulent behavior would be very demanding, especially for high Reynolds number flows, in terms of computational cost; therefore turbulence models are

often adopted instead of a complete turbulence simulation. Among turbulence models, the most diffused are certainly the approaches known as Reynolds Averaged Navier-Stokes (RANS) equations. In these models Navier-Stokes equations are averaged in time, then the flow is solved in terms of mean variables; indeed RANS adopt the Reynolds decomposition, in which each variable of interest is divided in an average part and a fluctuating part. Turbulence can be defined as statistically steady or statistically unsteady, in the latter case mean values are time dependent, while in the former one they are not. In case of statistically unsteady flows, then we should refer to the equations used as Unsteady Reynolds Averaged Navier-Stokes equations (URANS).

In order to adopt these equations, some strong assumptions have to be introduced, these hypothesis are usually not satisfied in real problems. However, this approach is often chosen because in some circumstances it is necessary to know only averaged or integral properties of the flow field. Moreover, RANS approach is significantly cheaper, in terms of computational cost, than DNS techniques, especially for high values of the Reynolds number of the flow.

Within RANS, there are many different models which tries to describe the turbulence, and two of the most diffused are the two-equations models $k - \omega$ (Wilcox et al. [1998]) and $k - \epsilon$. These methods describe the turbulence using two transport equations, the first one is in both cases an equation for the turbulent kinetic energy k, the second one can be either for the specific turbulence dissipation rate ω or for the turbulence dissipation rate ϵ. Models which introduce the definition of turbulent kinetic energy ask for the adoption of a modified energy equation in which the total energy has to include also the turbulent kinetic energy. An alternative is to add a new source term to the classical energy equation. Among two equations models, $k - \epsilon$ is the more reliable but is not particularly suitable for fast rotating flows, while $k - \omega$ is often adopted for aerospace applications. Another largely diffused approach is the one-equation Spalart-Allmaras model (Spalart and Allmaras [1994]), which is often adopted for the analysis of transonic or supersonic flows. Indeed, this model provides very good results for fully turbulent high Reynolds number flows.

An alternative approach also exists, which tries to solve the real flow instead of the averaged one, it is called LES (Large Eddy Simulation). In this kind of simulation governing equations are derived by "filtering" the Navier-Stokes equations. Resultant filtered equations contain terms which account for the effects of the scales deleted by the filter, and the resultant flow field is essentially the flow field restricted to the components that can be solved by the adopted mesh. LES are not well suited for the analysis of flow around solid bodies with high values of Reynolds number (external aerodynamics) because of the large number of cells required near the walls.

2.3.3 Boundary conditions

In order to have a complete analysis of the flow field, boundary conditions should be imposed. In Euler equations, wave propagation effects are considered and they are described by the characteristic signals, these signals are transported along characteristic lines. At inlet and outlet boundaries, some of the information needed are taken from the computational domain and some are given by the external environment, through the imposition

of BCs. The number of boundary conditions that have to be imposed depends on the number of characteristic lines which enter in the computational domain. For example, if subsonic flows are considered, $n-1$ boundary conditions have to be imposed at the inlet, where n is the number of flow variables, and one quantity is imposed at the outlet. Things changes while considering supersonic flows, in this case n conditions have to be imposed at the inlet, and no BCs are imposed at the outlet.

In the presence of diffusive effects, which are considered in the Navier-Stokes equations, other boundary conditions should be added to the ones imposed for the Euler equations. BCs should be introduced, in particular, near the solid walls, where the no-slip condition is usually imposed on momentum variables. As written before, when Reynolds Averaged Navier-Stokes equations are adopted, new variables have to be introduced, such as the turbulent kinetic energy k. Usually experimental data are not available for these variables and empirical correlations have to be introduced in the model in order to link the known data about BCs and the variables adopted in the turbulence model.

2.3.4 Immersed boundary methods

Interesting methods that can be applied in full CFD resolutions are the Immersed Boundary (IB) methods which have been introduced by Peskin [1972], who adopted these techniques for biomedical purpose, in particular for the analysis of cardiac mechanics and blood flow. IB methods are discussed in Mittal and Iaccarino [2005]. These methods simulate viscous flows with immersed boundaries while adopting Cartesian grids that do not conform to the shape of these boundaries, thus a new way of introducing the effects of the IB in the flow analysis has been developed.

The conventional approach in simulating a flow past a solid body would adopt structured or unstructured grids which conform to the body, while in IB methods the boundary is represented by a surface grid and a Cartesian volume grid non conformal to the body is generated without regard to the surface grid. The equations describing the flow-field have to be modified in the proximity of the solid boundary in order to incorporate the BCs in the Cartesian volume grid, then governing equations are discretized with a finite differences, finite volumes or finite elements method.

There are some advantages and disadvantages in the adoption of an Immersed Boundary method instead of following the conventional approach. First of all, the generation of the grid is clearly much simpler if IB methods are chosen, and this leads to significant advantages in terms of time expense and computational cost. Anyway, this grid has to provide sufficient resolution at any location. Among the disadvantages, it should be observed that imposing the boundary conditions, when adopting IB methods, is not trivial. Moreover, while utilizing body-conformal grids, a better control of the grid resolution in the proximity of the body is provided.

For these reasons methods adopting body-conformal grids are very useful when complex geometries are concerned, but it should be considered that a deterioration in grid quality is observed when complexity of the geometry is increased. When considering fluxes with moving boundaries, such as the flow around an aeronautical propeller, adopting a body-conformal grid will require the generation of a new grid at each time step. This can clearly lead to an increase in computational cost, and has a negative impact on simplicity

and accuracy of the resolution method. In contrast, immersed boundary methods are widely used for the analysis of flows with rotating boundaries, because the introduction of body motion in these methods is quite simple thanks to the adoption of a stationary, non-deforming Cartesian grid.

2.4   The Actuator Disk Method (ADM)

The lack of accuracy of the Blade Element Momentum Theory (BEMT) and the high computational cost and time expense of high fidelty full CFD simulations, have brought researchers to investigate the possible introduction of new methods, which could guarantee a good level of reliability with a limited computational cost. Different methods have been developed along the years and most of them has followed the idea of approximating the propeller as a time-averaged source of momentum which is used as source force in 3D CFD flow simulations. In most of them, source terms are based on the Momentum Theory.

The Momentum Theory introduced in the previous chapters is a simple concept which can be adopted for a first evaluation of propellers' performance. However, this concept can also enable us to introduce a discontinuity in governing flow equations. As in momentum theory, the propeller is modelled as a permeable disk which surface is normal to the free-stream velocity, and forces exchanged between the disk and the flow are evenly distributed on the surface. An early formulation of the Actuator Disk Method (ADM) has been introduced by Wu et al. [1962], who applied this technique to the analysis of heavily loaded propellers. In its classical formulation, ADM solve the flow field by means of the unsteady and axisymmetric Navier-Stokes equations, which means that the only assumption made is that of axisymmetric flow, still necessary in this method. There have been many improvements of the method along the years, which have come from many different works. The Actuator Disk Method version that we consider in this thesis is the one developed by Sørensen and Myken [1992].

They proposed a method in which a finite difference solution of unsteady, axysimmetric Euler equations is adopted. Rotor blades are replaced by volume forces which are used as source terms in the flow equations, this allows to evaluate the influence of the rotor on the flow field. The solution of Euler equations is sought iteratively through a time stepping procedure, which assures time accurate results at each time step. Volume forces are estimated thanks to experimental two-dimensional airfoil data, but it has to be noted that this model is three-dimensional.

The flow is assumed as axisymmetric, inviscid and incompressible by Sorensen and Myken. With these assumptions, Euler equations are written in terms of cylindrical coordinates (x, r, θ), with corresponding velocity vector (u, v, w):

$$\frac{\partial(ur)}{\partial x} + \frac{\partial(vr)}{\partial r} = 0; \tag{2.39}$$

;

$$\frac{\partial u}{\partial t} + u\frac{\partial u}{\partial x} + v\frac{\partial u}{\partial r} = -\frac{1}{\rho}\frac{\partial p}{\partial x} + \frac{f_x}{\rho}; \tag{2.40}$$

$$\frac{\partial v}{\partial t} + u\frac{\partial v}{\partial x} + v\frac{\partial v}{\partial r} - \frac{w^2}{r} = -\frac{1}{\rho}\frac{\partial p}{\partial r} + \frac{f_r}{\rho}; \tag{2.41}$$

$$\frac{\partial w}{\partial t} + u\frac{\partial w}{\partial x} + v\frac{\partial w}{\partial r} + \frac{vw}{r} = \frac{f_t}{\rho}. \tag{2.42}$$

These equation are, respectively, continuity equation and momentum balance along x, r and θ directions. p is the pressure, ρ is the air density, t is the time and f is the vector containing the three components of the volume force acting on the rotor. To solve the system, boundary conditions and initial conditions should be introduced; boundary conditions are imposed at the inflow, at the outflow, along lateral boundaries and along symmetry axis; while at time $t = 0$ the flow is assumed to have a perfectly axial direction. We should also remember that the force field and the kinematics are coupled, and the solution has to be obtained iteratively. If the intention is to keep the computational cost under a certain level, mesh dimensions should be reduced as much as possible, but obviously without introducing strong wall effects in the simulation.

The solution of the continuity equation can be obtained employing a second-order accurate central-difference discretization; while because of the hyperbolicity of the momentum balance equations, they are solved with a first-order accurate upwind discretization.

The Actuator Disk Method has become very popular and constitutes a quite reliable and computationally cheap method of evaluating the flow across a propeller. Indeed, it has now been applied to the analysis of aeronautical propellers for years. However, the main limitations of this method are represented by the assumption of axis-symmetric flow and by the fact that the disk is assumed as uniformly loaded. These weaknesses have led to the introduction of an alternative method which tries to distribute the loading only on lines representing the propeller blades, rather than on a disk representing the propeller.

Chapter 3

The Actuator Line Method (ALM)

The axisymmetric assumption is the most critical part of the Actuator Disk Method because, as it can be easily seen, forces acting on a propeller are exchanged only between the propeller blades and the flow, and consider them as evenly distributed on a disk is a quite strong approximation. For this reason Sorensen and Shen [2002] decided to introduce an alternative model, known as Actuator Line Method (ALM), which combines a 3D Navier-Stokes solver with a technique that distributes forces over lines representing the blades. Kinematics of the wake is resolved thanks to Navier-Stokes equations while acting forces are included in the momentum balance using tabulated airfoil data. In the model proposed by Sorensen the flow is essentially inviscid and the viscous effects from the boundary layer are introduced as integrated quantities. This method has been introduced and validated for the analysis of wind turbines, performing comparisons between ALM, ADM and high fidelity CFD simulations, a very good agreement with full CFD resolutions has been showed. Later works by Ravensbergen et al. [2020] and Churchfield et al. [2017] also contributed to assure the reliability of the Actuator Line Method.

As written before, the goal of this thesis is to implement the ALM for the analysis of an aeronautical propeller, and evaluate its reliability through the application of the method to a relevant case study.

3.1 Numerical model

The physical model adopted in order to solve the fluid-dynamics are the compressible Navier-Stokes equations which are recalled in the following lines:

$$\frac{\partial \rho}{\partial t} + \nabla * (\rho \vec{V}) = 0; \tag{3.1}$$

$$\frac{\partial \rho \vec{V}}{\partial t} + \nabla * (\rho \vec{V} \vec{V}) = -\nabla(p) + \nabla * (\tau) + \rho \vec{f_e}; \tag{3.2}$$

$$\frac{\partial \rho E}{\partial t} + \nabla * (\rho \vec{V} E) = -\nabla * (p\vec{V}) + \nabla * (\tau * \vec{V}) + \rho \vec{f_e} \vec{V}. \tag{3.3}$$

Where the first equation is the mass balance, the second equation is the momentum balance, which can be divided in three differential equations along axis x, y and z, and the last one is the energy balance. In these equations, the term $\vec{f_e}$ represents the volume forces which are calculated thanks to the actuator line model and then introduced in Navier-Stokes equations as momentum source terms. τ is the shear-stress tensor and its components are computed as:

$$\tau_{ij} = \mu(\frac{\partial u_i}{\partial x_j} + \frac{\partial u_j}{\partial x_i}) - \frac{2}{3}\delta_{ij}\nabla * \vec{V}. \tag{3.4}$$

Where clearly $\vec{x} = [x \quad y \quad z]$ and $\vec{u} = [u \quad v \quad w]$; and μ is the dynamic viscosity. The term δ_{ij} is equal to zero if $i \neq j$, and equal to 1 if $i = j$.

The object of this thesis has been the calculation of the source forces through the implementation of a function based on the ALM, and a comprehensive description of the strategies adopted will be provided in section 3.2. These source terms have been later introduced in a CFD code which has performed the resolution of the Navier-Stokes equations. A far more exhaustive description of the code used for the simulations can be found in bibliography (Ferrero [2014]).

In the computational fluid-dynamics analysis here described all the variables of the Navier-Stokes equations have been divided for conventional reference values and used in their non-dimensional form. In the present work time integration is performed by utilizing an explicit Runge-Kutta method of the first order, while the spatial discretization is made employing a Discontinuous Galerkin (DG) method of the second order.

DG methods have some features in common with both finite volumes (FV) methods and finite elements (FE) methods, and they combine some of the advantages of these two techniques, for this reason they are vastly adopted for the numerical resolution of Navier-Stokes equations. Various numerical fluxes from FV methods have been inherited by DG methods, however, there is still one remarkable difference between these discretization methods. Indeed, in finite volumes methods, only the average values of the conservative variables are known inside the cells, while in DG methods a large number of degrees of freedom is introduced inside the element and this feature helps to simplify high-order reconstructions, because all the needed information is already contained in the element. This is the feature that DG methods and finite elements methods have in common.

In order to close the equations, boundary conditions should be imposed at the inflow, at the outflow, and along lateral boundaries.

In the first phase, we had to evaluate the affordability of the method with relatively fast simulations, so we adopted a small cubic mesh which side measures 4 meters, with 40 cells on each side, for a total of 68921 nodes; a mesh of these dimensions can introduce wall effects and for more accurate results a bigger mesh should be adopted. Indeed, after this first phase, a larger cubic mesh has been adopted, which side measures 16 meters. Three different levels of resolution have been adopted, a less refined mesh with 40 cells per side, for a total amount of 68921 nodes; a moderately refined mesh with 80 cells per side, for a total amount of 531441 nodes; and an highly refined mesh with 160 cells per side,

bringing the total amount to 4173281 nodes. With this last mesh in particular, the time expense grows up significantly, but it is still lower than the time that would be required by a full CFD resolution.

3.2 Computation of body forces

As written before, the true object of this thesis have been the calculation of the source forces which have to be introduced in the Navier-Stokes equations. Source terms of the forces exchanged between the propeller and the flow have been obtained according to the Actuator Line Method (ALM). This method has been introduced by Sorensen and Shen [2002] and it has been used in many later works, for example by Ravensbergen et al. [2020]. At first it had been studied in order to be applied in the project and analysis of wind turbines, but it also can be useful for other interesting applications, such as analysis of propellers or helicopters' rotors. This method calculates the body forces through a series of steps, resumed in the following lines.

For the implementation of the ALM we have written a subroutine in FORTRAN, which has been later introduced in a CFD code implementing the resolution of N-S equations. Given x, y, z, t, ρ, u, v and w as input parameters of our function, we need to compute forces acting on the flow by means of the Actuator Line Method. Input values x, y and z are the spatial coordinates while t is the time coordinate, ρ is the flow density, u, v and w are the absolute velocity components. It is necessary to establish a reference system related to the propeller. The origin will be set at the centre of the propeller and x will be positive in the stream direction, positive directions for y and z axis can be found following the right-hand rule.

As the very first step we need to know if the point (x, y, z) touches one of the blades at the time t; if not, then the force will be equal to zero. We assume that the blade is vertical at time $t = 0$ and we compute the angle between the blade and the vertical axis at time t as $\theta = \omega t$, where ω is the rotational velocity of the propeller; we also assume θ to be positive in clockwise direction while the propeller is seen from upwind. If the propeller has more than one blade, which happens nearly always, all the following calculations are iterated for other values of theta; indeed, the number of blades can be introduced as a parameter, at the beginning of the subroutine. As a first approximation we have considered each blade as a cylinder whose height equals the radius of the blade and which basis has c (chord of the blade's profile) as diameter; the following description of the resolution method will be based on this approximation. We need to know if the point in input falls inside the circle described by the rotation of the blade, which is true only if $\sqrt{y^2 + z^2} \leq R$, where R is the radius of the blade. Then we have computed the distance between the point and the straight line which coincides with the axis of the blade, if this distance is lower than $\frac{c}{2}$ the point is located on the blade.

In order to calculate this distance, we firstly had to write the equation of the straight line. This could be done by knowing that this line is passing through two points, which are the centre of the propeller $(0, 0, 0)$, and the point of the axis of the cylinder which is at the tip of the blade at time t: $(0, -R \sin \theta, R \cos \theta)$. The equation of the straight line

results to be:

$$x = 0; \tag{3.5}$$

$$z = -\frac{y}{\tan \theta}. \tag{3.6}$$

Which, if written in parametric form, becomes:

$$x = 0; \tag{3.7}$$

$$y = t; \tag{3.8}$$

$$z = -\frac{t}{\tan \theta}. \tag{3.9}$$

Thus, the direction vector will result to be: $\vec{r} = \begin{bmatrix} 0 & 1 & -\frac{1}{\tan \theta} \end{bmatrix}$.

It is also useful to compute the versor $\vec{e_r} = \frac{\vec{r}}{\|\vec{r}\|}$; then the distance between the point and the straight line can be easily computed: it is the norm of the vectorial product between this versor and the vector which gives the position of the point with respect to the origin of the axis, which is so: $\begin{bmatrix} x & y & z \end{bmatrix}$. As said before, if this distance is lower than $\frac{c}{2}$ we can go on with the rest of the calculations, otherwise the forces will simply be equal to zero.

Propeller blades are divided into a certain number of discrete elements (20 in our case) and an actuator point is located at the centre of each element. If the point in input touches one of the blades, then it is possible to determine precisely, with a simple calculation, which one of the elements is touched. After that, a certain value of r can be chosen properly for the given point, where r is the radial coordinate of the actuator point at the centre of the element considered.

An important variable of our problem is the fluid velocity relative to the rotating blade, that we can compute as:

$$V_{rel} = \sqrt{u_{rel}^2 + v_{rel}^2}. \tag{3.10}$$

The relative velocity components are given by the combination of the fluid velocity and the rotational component given by the propeller, and can be written as follows:

$$u_{rel} = u; \tag{3.11}$$

$$v_{rel} = -\omega r + v \cos \theta + w \sin \theta. \tag{3.12}$$

It can be useful to remind that u, v and w are the absolute velocity components, ω is the rotational velocity of the propeller, θ is the angle between the blade and the vertical axis at time t and r is the radial coordinate of the actuator point. It should be also noted that these relative velocity components are located in a reference frame which is rotating according to the propeller's blade, u_{rel} is directed in the axial direction while v_{rel} is directed in the tangential direction.

Knowing the relative velocity components allows us to compute the angle that the relative velocity makes with the rotor plane, which is called the flow angle, ϕ and is determined as:

$$\phi = \arctan \frac{u_{rel}}{v_{rel}}. \tag{3.13}$$

Then the angle of attack can be written as $\alpha = \phi + \gamma$, being γ the local pitch angle of the blade. The α just defined is the geometric angle of attack, which is the angle between the chord line and the free-stream direction, and it coincides with the aerodynamic angle of attack (or simply angle of attack, AOA) only for symmetrical airfoils. Indeed, the angle of attack is defined as the angle between the zero-lift line and the free-stream velocity and for asymmetrical airfoils the zero-lift line is rotated of an angle α_0 with respect to the chord of the profile. So, if we have to consider an asymmetrical airfoil, the correct definition of the angle of attack α will be:

$$\alpha = \phi + \gamma - \alpha_0. \tag{3.14}$$

A simple representation of the reference frame adopted for the definition of the considered angles is reported in figure 3.1.
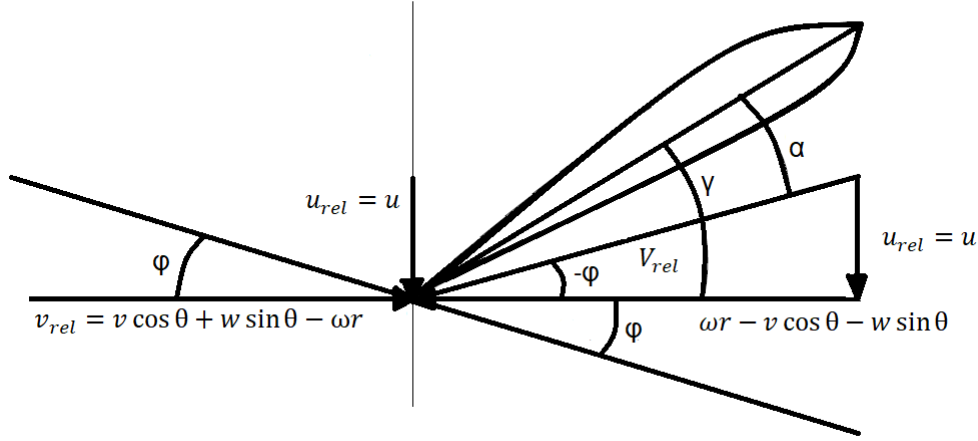
Figure 3.1.   Velocity components acting on the blade element.

The computed angle of attack could be used along with the local Reynolds number to obtain lift and drag coefficients, but in this implementation of the method we can assume to have constant C_D and $C_{L\alpha}$ and so calculate the lift coefficient as $C_L = C_{L\alpha}\alpha$.

Lift and drag forces per unit length are computed using the well-known formulas:

$$L = \frac{1}{2}\rho V_{rel}^2 c C_L; \tag{3.15}$$

$$D = \frac{1}{2}\rho V_{rel}^2 c C_D. \tag{3.16}$$

Where ρ is the fluid density and c is the chord of the blade's profile. Lift and drag must be rotated in order to obtain an axial force F_X and a tangential force F_T, force along the radial direction of the blade has zero magnitude. These are still forces per unit length, so

they have to be multiplied by the spacing between the actuator points to obtain a force expressed in Newton. We have:

$$F_X = (L \cos\phi + D \sin\phi)\frac{R}{NC}; \tag{3.17}$$

$$F_T = (L \sin\phi - D \cos\phi)\frac{R}{NC}. \tag{3.18}$$

R is the radius of the blade, while NC is the number of discrete elements in which the blade has been previously divided.

As for the last step of this method, the aerodynamic force acting on the flow due to the blade element is obtained combining axial and tangential forces computed before, and is then divided into three components acting along directions x, y and z:

$$F_1 = FX; \tag{3.19}$$

$$F_2 = FT \cos\theta; \tag{3.20}$$

$$F_3 = FT \sin\theta. \tag{3.21}$$

It is useful to remind that we have assumed that the blade makes an angle θ with the vertical axis, and the propeller rotates clockwise when seen from upstream. Since the outputs of our function are the source terms of the aerodynamic force acting on the flow, we compute these terms dividing the force components by the volume of the blade element, which is given by:

$$Vol = \pi\frac{c^2}{4}\frac{R}{NC}. \tag{3.22}$$

Another term has been added for the calculation of the torque acting on the blade element considered, which is calculated as:

$$TQ = -F_t r. \tag{3.23}$$

This term has also been divided by the volume of the blade element. Source forces acting on each element of the blades, along the three directions, have been integrated to obtain the total forces exchanged between flow and propeller, along directions x, y, z at a certain time. The integration has been performed at each time step, and the same thing has been done for source torque. Thanks to this integration we had obtained the thrust produced at each time step, which coincides with force acting along direction x, and also the torque acting on the propeller.

Part II

Numerical results

Chapter 4

Case study

4.1 Weick's propeller

The case study considered is the propeller projected by Weick and discussed in the study Weick [1930], it has also been analyzed by Tognaccini [2014], by means of the Blade-Element Momentum Theory (BEMT), which has shown a good agreement with the experimental data.

This propeller was tested in the Twenty-Foot Propeller Research Tunnel of the National Advisory Committee for Aeronautics, and it was mounted on a Wright "Whirlwind" J-5 engine. It is a three blades propeller with a radius of 1.587 meters, mounted on a hub with a diameter of 20 centimeters, and all the blades were set at a pitch angle of 15.5° at 75% of the radius. The distributions of chord and pitch angle along the radius are given, we can therefore choose a precise value of c and γ for each blade element. Blades were all made to fit the same hub and were made of aluminum alloy, and a representation of the single blade can be found in figure 4.1. We have assumed C_D and $C_{L\alpha}$ as constant parameters and the values chosen are, respectively, 0.020 and 2π. The variation of chord and pitch angle along radius is shown in figure 4.2, with pitch angle traced back to 0° at 75% of the radius (so we will have to add 15.5° to these values in order to have the real local pitch angle of the blades).

Experimental tests were conducted and for a set of different values of density ρ, velocity V_∞ and rotating velocity n gave a set of different values for thrust T and expended power P. These values were reduced to the well known coefficients of thrust C_T (2.2), power C_P (2.3) and propulsive efficiency η (2.4) and plotted against the advance ratio J (2.1). In these formulas D is the propeller diameter and n represent the revolutions per unit time ($round/s$). The coefficients are dimensionless, so that any homogeneous system of units can be adopted. Results are plotted in figure 4.3.

Tognaccini [2014] adopted the Blade Element Momentum Theory (BEMT) to determine the characteristic curves of the propeller proposed by Weick, this method has been implemented with a code written in FORTRAN. Since in the expressions for the calculation of C_T and C_P given by the BEMT, the only unknown quantity is the angle of attack α, three different methods for the determination of α have been introduced in this work.
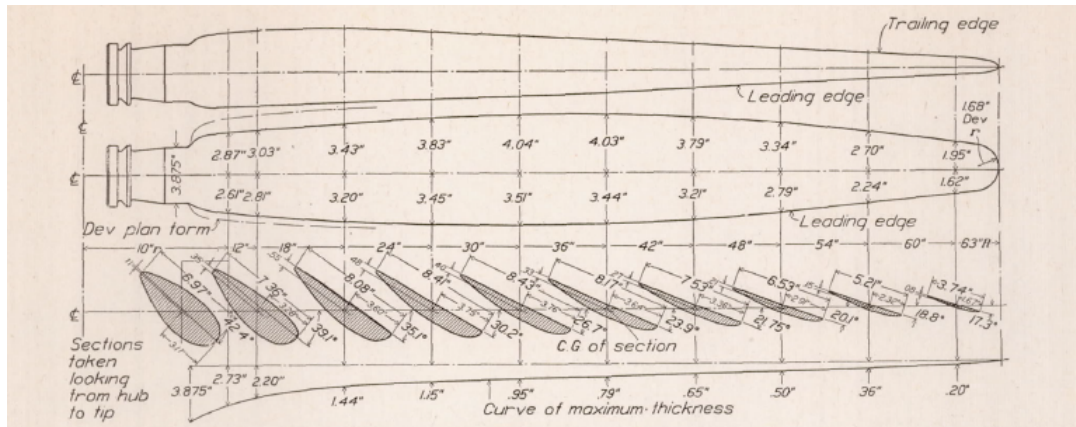
Figure 4.1.   Blade of 10.5 ft diameter propeller (Weick [1930]).
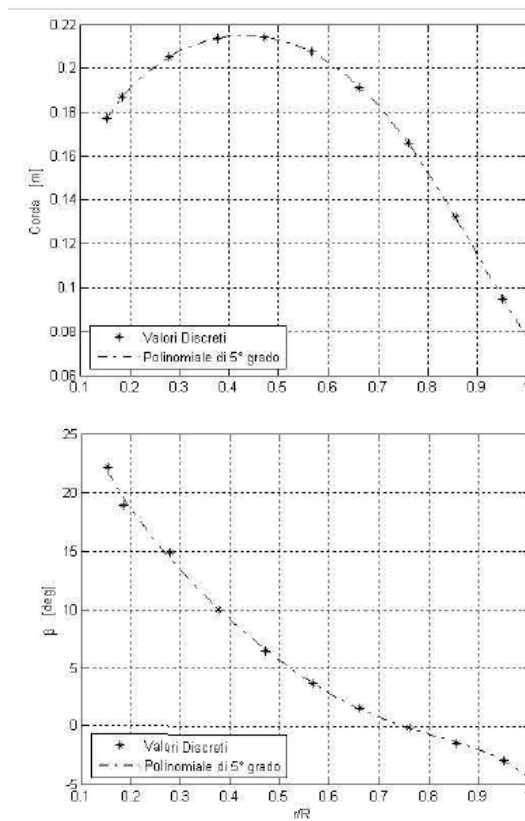

Figure 4.2.   Evolution of chord and pitch angle along radius (Tognaccini [2014]).

In this code a correction for the effects due to the finite number of blades, as well as a correction which accounts for radial velocity components, have been introduced. An interesting part of this research is that in the calculation the blades were set at five different values for pitch angle, varying from 20° to 40°. Results have shown a significant increase in thrust and power coefficients, for higher values of pitch angle. Moreover, with an increase in pitch angle, efficiency curves' maximum shifts to the right, and the highest level of efficiency is obtained for higher values of J. However, for high values of pitch angle and low values of J, results for thrust and power are not reliable because the Blade Element Theory does not account for stall conditions.
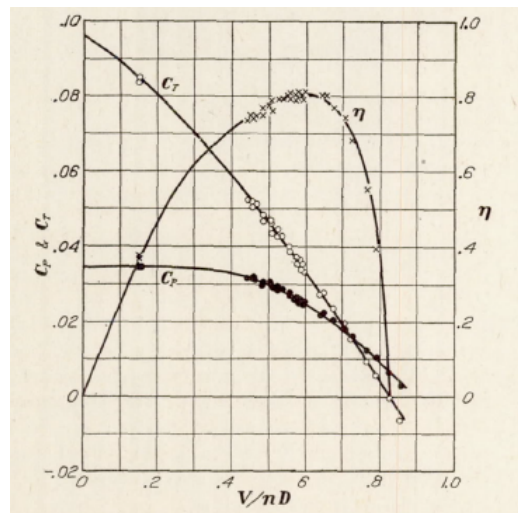
Figure 4.3.   Performance of Weick's propeller (Weick [1930]).

Chapter 5

Results and conclusions

In order to compare results obtained with this implementation of the actuator line method with experimental results, or even with results provided by other resolution methods, we have taken the force along x axis acting on the flow and the torque acting on the propeller.

Expended power has been calculated as:

$$P = \omega C. \tag{5.1}$$

Where ω is the rotational velocity expressed in rad/s. At this point, thrust coefficient, power coefficient and propeller's efficiency have been calculated following, respectively, formulas 2.2, 2.3 and 2.4; while the advance ratio has been calculated with formula 2.1.

As written before, in the first analysis we have used a relatively simple mesh, it's a cubic mesh which side measures 4 meters and it is composed by 68921 nodes. A mesh with a side dimension that is not so bigger than the diameter of the propeller, can introduce wall effects. However, this mesh can be adopted for a first evaluation about the reliability of the method, and more precise results can be obtained while using bigger meshes. Indeed, after these first simulations, a cubic mesh which side measures 16 meters has been adopted, with three different levels of resolution. A less refined mesh with 40 cells per side, for a total amount of 68921 nodes; a moderately refined mesh with 80 cells per side, for a total amount of 531441 nodes; and an highly refined mesh with 160 cells per side, bringing the total amount to 4173281 nodes.

A first comparison has been made to the results provided by Tognaccini [2014], who adopted a resolution method based on the Blade Element Momentum Theory (BEMT), which results are shown in figure 5.1 and 5.2, for five different values of pitch angle at 75% of the chord. In the figures continuous lines and dotted lines can be seen. Continuous lines show the results obtained with the first, less reliable, method adopted to calculate α; in this method small angles of attack are assumed and the axial induced velocity is assumed to be only function of the radial position on the blade. In the second method, the only assumption made was that of small angles of attack, while in the third method no simplifying hypothesis have been made. These two methods, more accurate, provided results very similar between them, which are plotted by the dotted line.

The actuator line method implemented, with this first grid adopted, has provided three different values of C_T and C_P for three different pitch angles ($20 \deg$, $30 \deg$ and

40 deg); all these results have been obtained for three different advance ratio: $J = 0.6537$, $J = 0.4358$ and $J = 0.3268$; which coincide with a rotational velocity of, respectively, $2000rpm$, $3000rpm$ and $4000rpm$. It should be noted that, even if Tognaccini suggested a reference value of $alfa0 = -3°$ for the analysis of Weick's propeller, in his implementation of the Blade Element Momentum Method he has adopted a simplifying assumption of symmetrical airfoils. Therefore we have adopted $\alpha_0 = 0°$ for this specific comparison. Values obtained have shown a good agreement as it can be seen in tables 5.1, 5.2 and 5.3. While graphical comparisons have been reported in figures: 5.3, 5.4, 5.5, 5.6, 5.7 and 5.8. We have plotted the evolution of C_T in time for pitch angle of 20° at 75% of the blade, and for a rotational velocity of $2000rpm$, and the results are showed in 5.9.

Results obtained for thrust coefficient have shown a good agreement with the ones provided by the method based on the BEMT. However, the comparison of values found for the power coefficient shows less precise results, especially for higher values of the pitch angle and for high rotational velocities. The overestimation of the power coefficient leads inevitably to an underestimation of the propeller's efficiency.
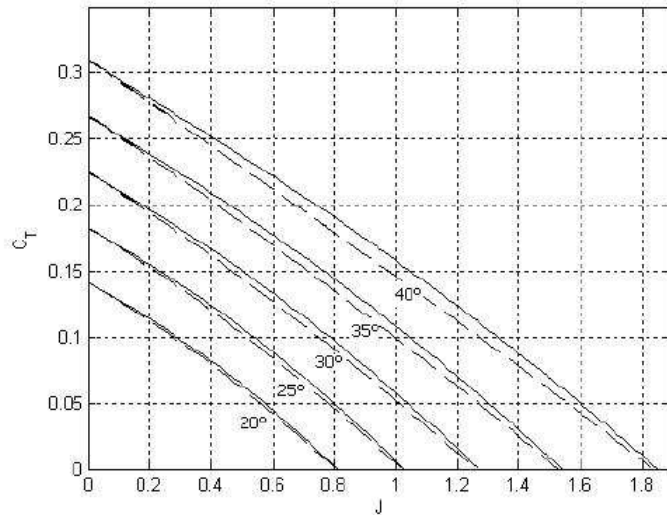
Figure 5.1.   Thrust coefficients obtained with BEMT (Tognaccini [2014]).

	$J = 0.6537$	$J = 0.4358$	$J = 0.3264$
CT BEMT	0.035	0.075	0.085
CT ALM	0.0315	0.0752	0.0772
CP BEMT	0.025	0.040	0.047
CP ALM	0.0287	0.0503	0.0490

Table 5.1.   Comparison between ALM and BEMT for $\gamma = 20$ deg.
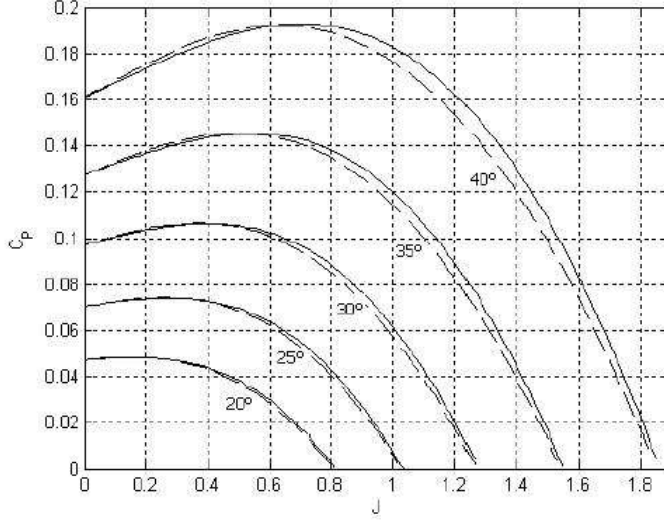
Figure 5.2.   Power coefficients obtained with BEMT (Tognaccini [2014]).

	$J = 0.6537$	$J = 0.4358$	$J = 0.3268$
CT BET	0.125	0.160	0.175
CT ALM	0.1237	0.1677	0.1840
CP BET	0.100	0.105	0.105
CP ALM	0.1106	0.1326	0.1454

Table 5.2.   Comparison between ALM and BEMT for $\gamma = 30$ deg.

Then the pitch angle has been brought to 15.5 deg, which is the value adopted by Weick [1930], so that we could compare actuator line method results with experimental data. The real airfoils were asymmetrical, so we have adopted a reference value of $\alpha_0 = -3°$, as suggested in bibliography (Tognaccini [2014]), and we have simulated the flow acting on the propeller. Simulations have been performed for three different values of advance ratio: $J = 0.6537$, $J = 0.4358$ and $J = 0.3268$; corresponding, respectively, to $n = 2000rpm$, $n = 3000rpm$ and $n = 4000rpm$. The results obtained with these simulations for the thrust coefficient have shown good agreement with experimental data, even with the small mesh adopted. However, also in this case, the results obtained for the power coefficient and for the efficiency are less accurate, especially for rotational velocities of $3000rpm$ and $4000rpm$. Results are shown in comparison with experimental data in figures 5.10, 5.11 and 5.12.

As written before three other meshes were also adopted, all these meshes were cubical with a side of 16 meters, the less refined one had 40 cells per side, the second one had 80 cells per side, while the one with the highest resolution had 160 cells per side. Obviously the time required for the simulations increases for a mesh with a larger number of nodes.

43

	$J = 0.6537$	$J = 0.4358$	$J = 0.3268$
CT BET	0.215	0.245	0.270
CT ALM	0.2200	0.2641	0.3011
CP BET	0.195	0.190	0.180
CP ALM	0.2225	0.2477	0.2621

Table 5.3.   Comparison between ALM and BEMT for $\gamma = 40 \deg$.
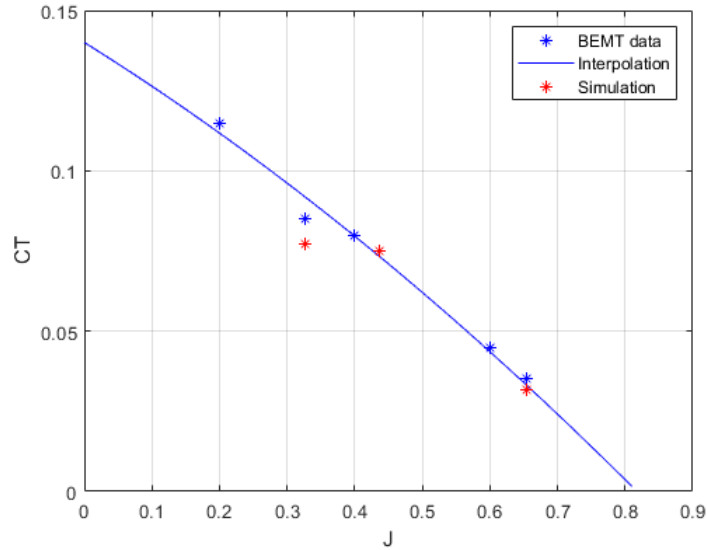
Figure 5.3.   Comparison between BEMT and ALM resolutions for CT ($\gamma = 20°$ at 75% of the blade).

We evaluated results given by the three simulations and compared them with experimental data in figures 5.13, 5.14 and 5.15.

In order to evaluate the influence of domain dimensions on the accuracy of results, a comparison has been made between results obtained for the mesh which side measures $4m$ and the one which side measures $16m$. The comparison has been made with the same level of mesh refinement, which means 40 cells per side for the small mesh, and 160 cells per side for the bigger one. Results are shown in figures 5.16, 5.17 and 5.18. This comparison has shown that, in this case, wall effects introduced by the little mesh are very small, and results obtained with the two different meshes are very similar. Of course, this observation should not be considered valid in general; but we have found that, for this case study, while adopting the implemented method, the effects of domain boundary are relatively weak.

VisIt (Childs et al. [2012]) allows to visualize the evolution of variables such as entropy or vorticity in the flow around a propeller. In figure 5.19 a visual representation of vorticity
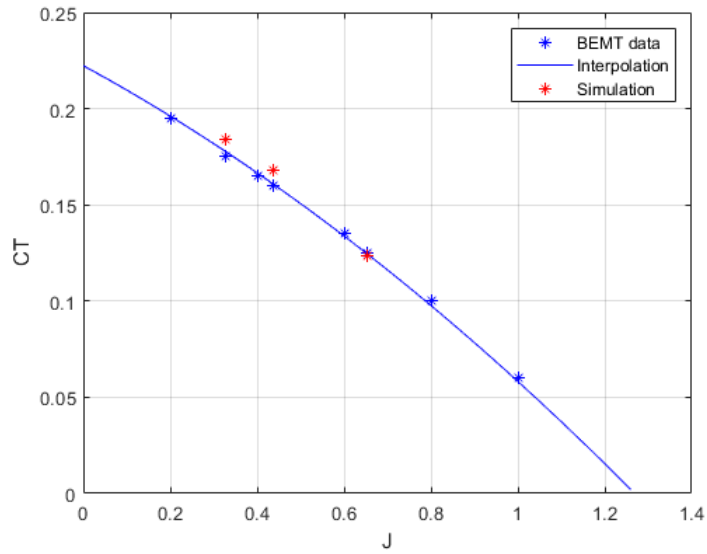
Figure 5.4.   Comparison between BEMT and ALM resolutions for CT ($\gamma = 30°$ at 75% of the blade).
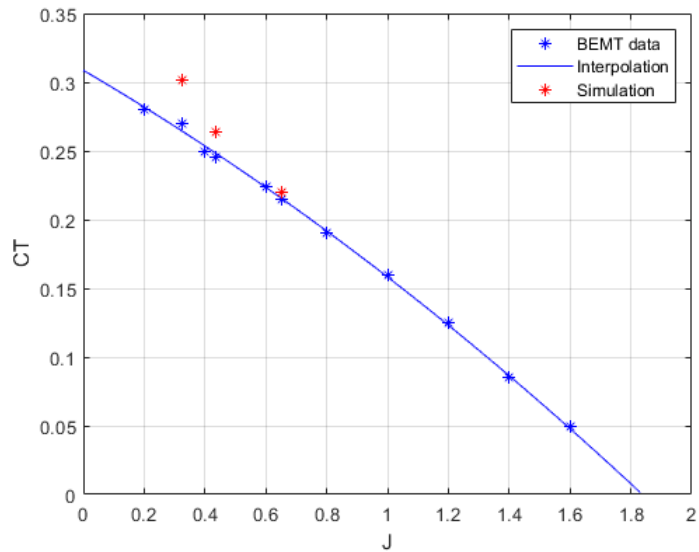
Figure 5.5.   Comparison between BEMT and ALM resolutions for CT ($\gamma = 40°$ at 75% of the blade).

after some time steps is provided, this representation is the result of a simulation conducted for the propeller considered with the bigger and most refined among the meshes adopted.
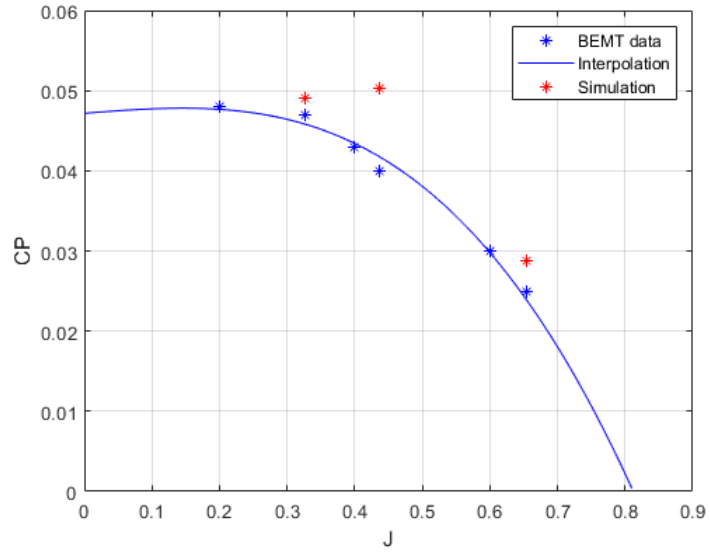
Figure 5.6.   Comparison between BEMT and ALM resolutions for CP ($\gamma = 20°$ at 75% of the blade).
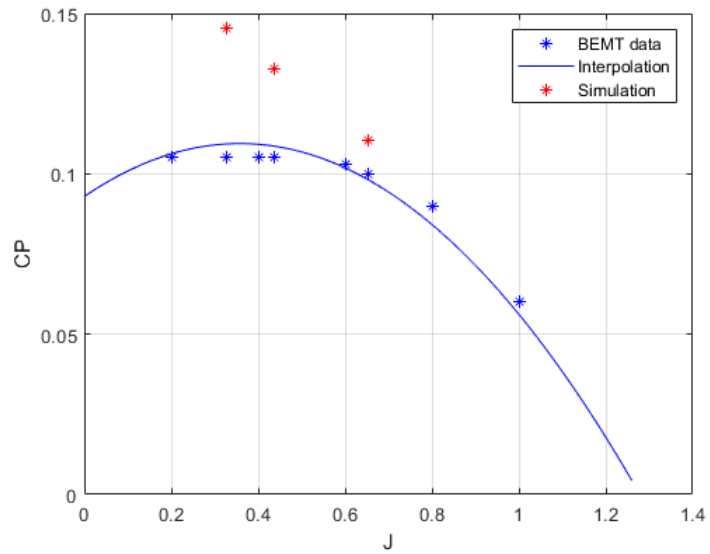
Figure 5.7.   Comparison between BEMT and ALM resolutions for CP ($\gamma = 30°$ at 75% of the blade).

Tip vortices introduced in the wake by the interaction between flow and propeller can be distinctively seen in this representation.
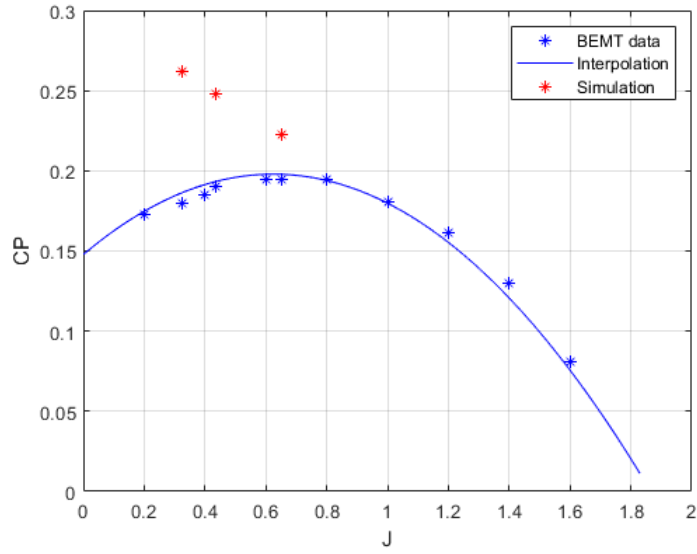
Figure 5.8. Comparison between BEMT and ALM resolutions for CP ($\gamma = 40°$ at 75% of the blade).
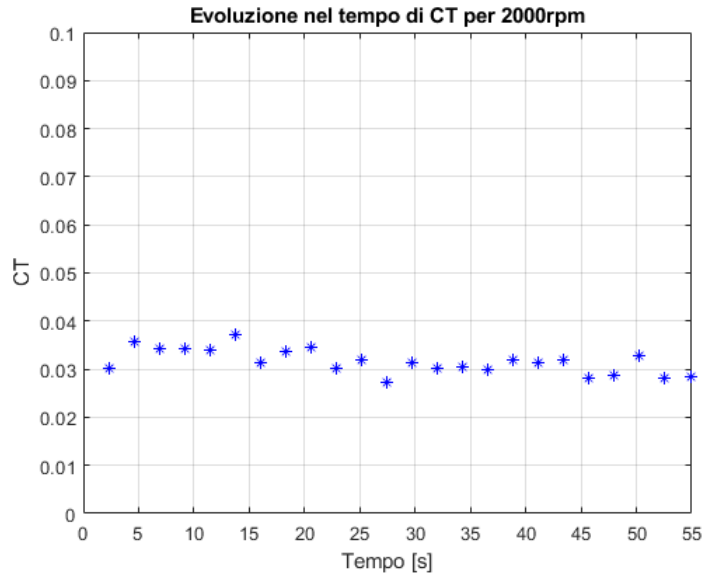
Figure 5.9. Evolution of C_T in time for $\gamma = 20°$ at 75% of the blade, and for $n = 2000rpm$.

In conclusion, the implemented Actuator Line Method has proven himself as reliable and with a relatively reduced computational cost. Future improvements to the method
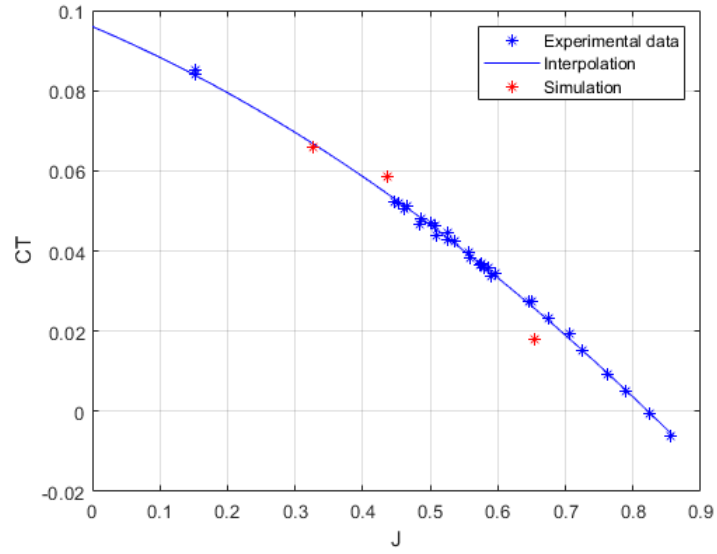
Figure 5.10. Comparison between experimental data and simulation results for CT ($\gamma = 15.5°$ at 75% of the blade).
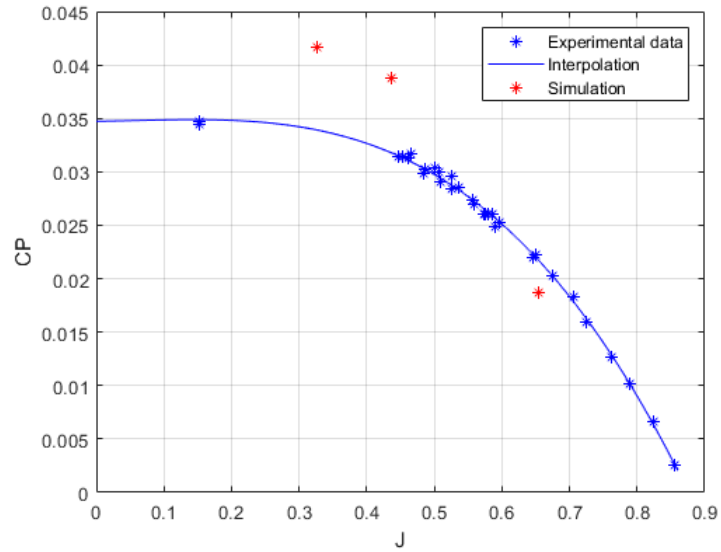
Figure 5.11. Comparison between experimental data and simulation results for CP ($\gamma = 15.5°$ at 75% of the blade).

could provide even more accurate results, especially for the evaluation of the power co-efficient. Comparisons between different meshes have shown that mesh refinement has

48
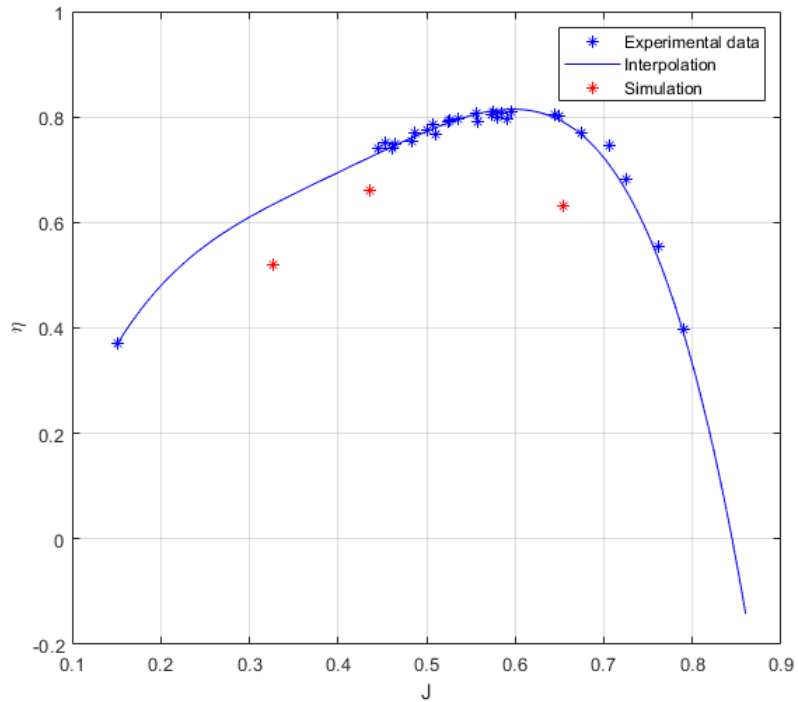
Figure 5.12.   Comparison between experimental data and simulation results for efficiency ($\gamma = 15.5°$ at 75% of the blade).

a relevant influence on accuracy. A possible strategy could be the adoption of a mesh with a side which measures less than $16m$ but big enough to assure the avoidance of wall effects, this mesh could be locally refined in the region of interest without causing a relevant increase in computational cost. Another strategy could involve the subdivision of the blades in a larger number of elements, while always choosing a precise value of chord and pitch angle for each blade element.
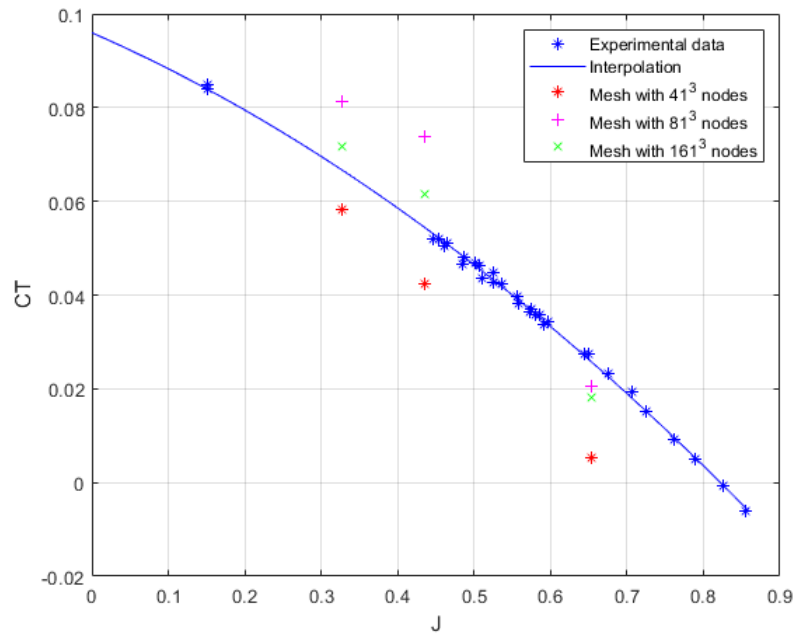
Figure 5.13.   Comparison between results derived with three different cubical meshes with a side of 16 meters for CT ($\gamma = 15.5°$ at 75% of the blade).
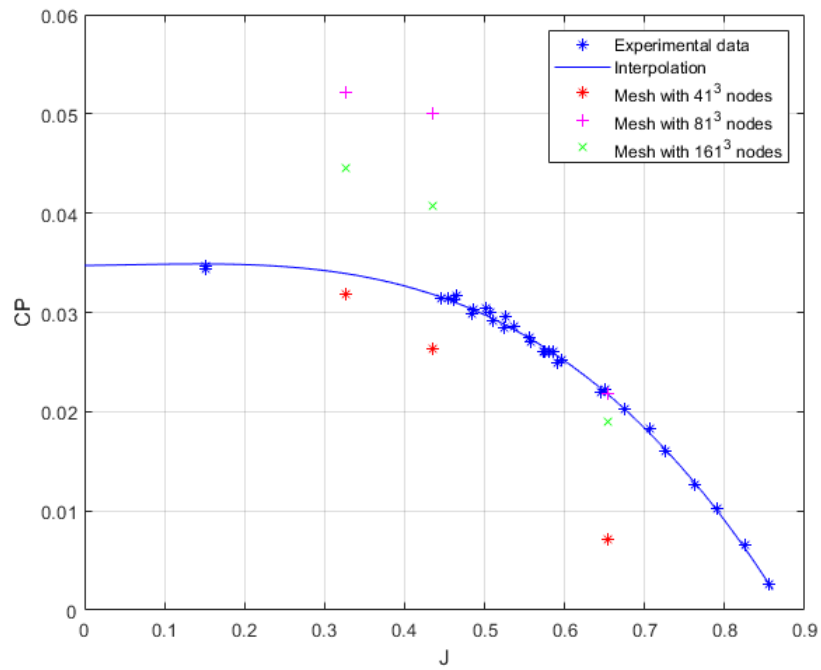
Figure 5.14. Comparison between results derived with three different cubical meshes with a side of 16 meters for CP ($\gamma = 15.5°$ at 75% of the blade).
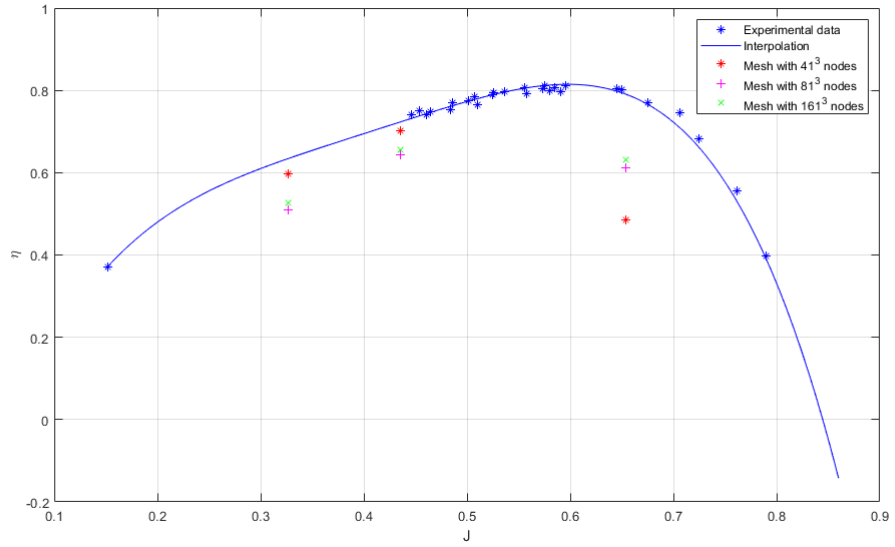
Figure 5.15. Comparison between results derived with three different cubical meshes with a side of 16 meters for η ($\gamma = 15.5°$ at 75% of the blade).
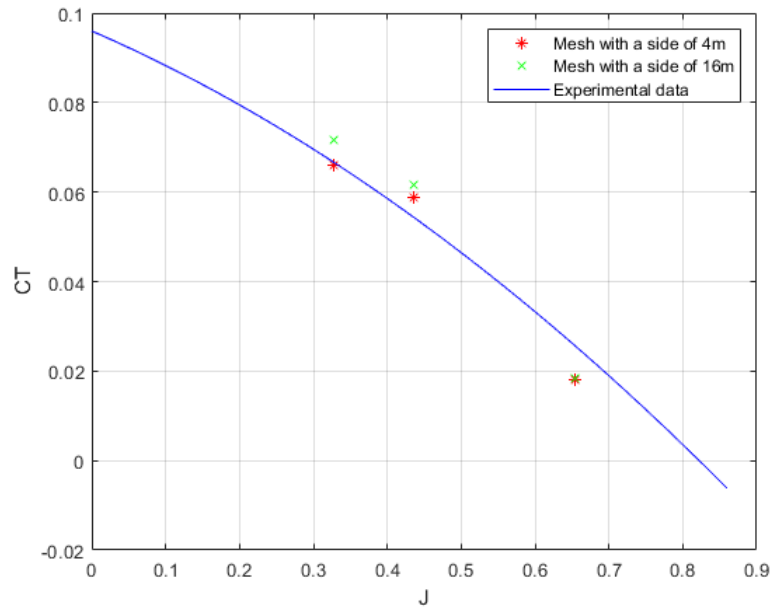
Figure 5.16. Comparison between results obtained with two meshes with different dimensions and same refinement for CT ($\gamma = 15.5°$ at 75% of the blade).
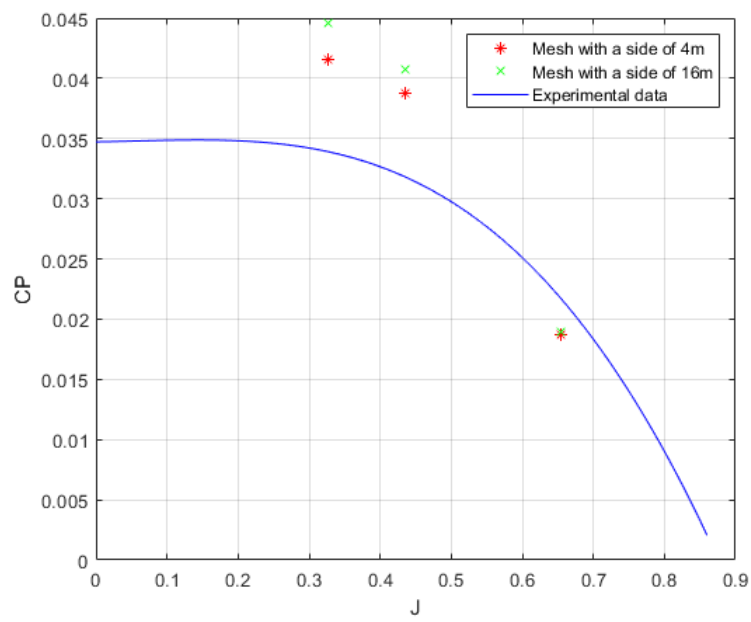
Figure 5.17.   Comparison between results obtained with two meshes with different dimensions and same refinement for CP ($\gamma = 15.5°$ at 75% of the blade).
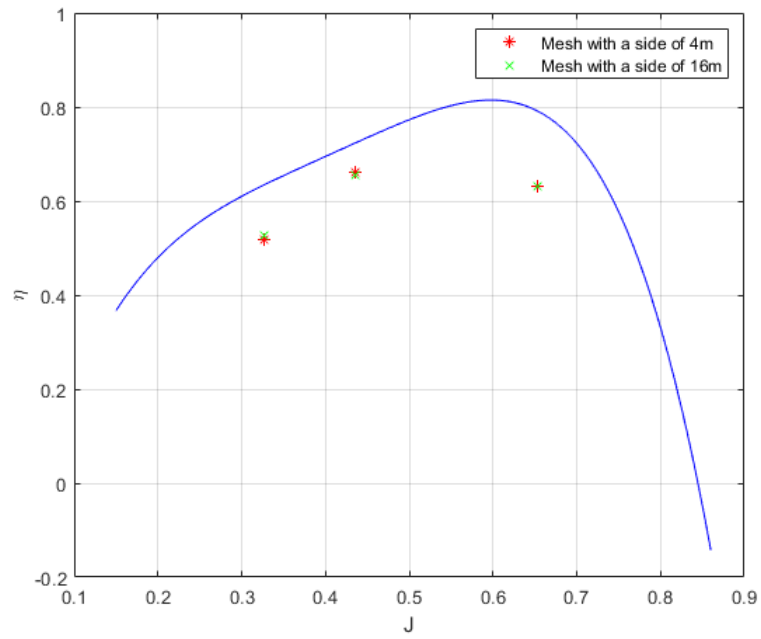
Figure 5.18.   Comparison between results obtained with two meshes with different dimensions and same refinement for η ($\gamma = 15.5°$ at 75% of the blade).
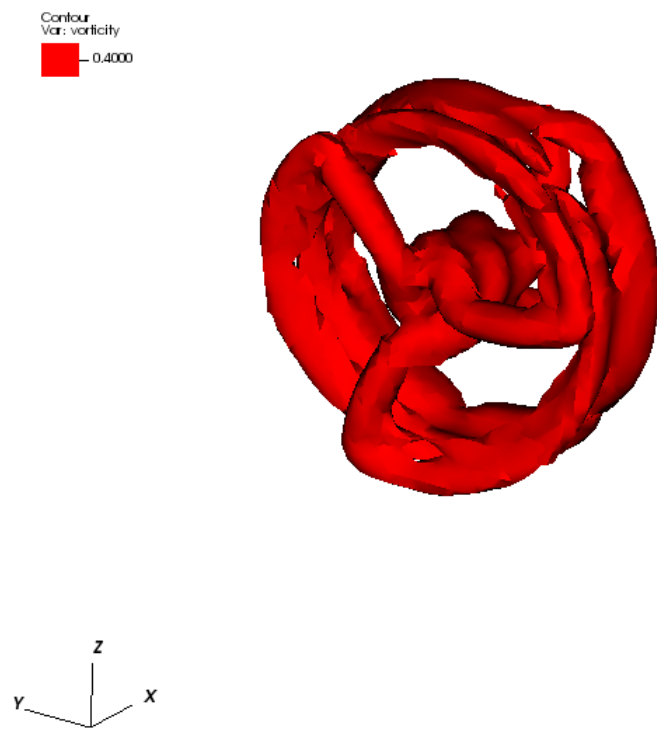
Figure 5.19.   Vorticity around a propeller rotating at $4000rpm$.

Bibliography

Albert Betz. Development of the inflow theory of the propeller. Technical report, 1920.

Joseph Ray Carroll. *Time-averaged surrogate modeling for small scale propellers based on high-fidelity CFD simulations*. Mississippi State University, 2013.

Hank Childs, Eric Brugger, Brad Whitlock, Jeremy Meredith, Sean Ahern, David Pugmire, Kathleen Biagas, Mark Miller, Cyrus Harrison, Gunther H. Weber, Hari Krishnan, Thomas Fogal, Allen Sanderson, Christoph Garth, E. Wes Bethel, David Camp, Oliver Rübel, Marc Durant, Jean M. Favre, and Paul Navrátil. Visit: An end-user tool for visualizing and analyzing very large data. In *High Performance Visualization–Enabling Extreme-Scale Scientific Insight*, pages 357–372. October 2012. doi: 10.1201/b12985.

Matthew J Churchfield, Scott J Schreck, Luis A Martinez, Charles Meneveau, and Philippe R Spalart. An advanced actuator line method for wind energy applications and beyond. In *35th Wind Energy Symposium*, page 1998, 2017.

Stefan Drzewiecki. *Théorie générale de l'hélice: hélices aériennes et hélices marines*. Gauthier-Villars et cie., 1920.

Domenic D'Ambrosio and Manuel Carreño Ruiz. Cfd simulation of propellers: Best practices analysis. 2019.

Andrea Ferrero. Computational fluid dynamics for aerospace propulsion systems : an approach based on discontinuous finite elements / andrea ferrero ; rel. francesco larocca, 2014.

Robert Edmund Froude. On the part played in propulsion by differences of fluid pressure. *Trans. Inst. Naval Architects*, 30:390, 1889.

Hermann Glauert. *The elements of aerofoil and airscrew theory*. The University Press, 1926.

Eric Vargas Loureiro, Nicolas Lima Oliveira, Patricia Habib Hallak, Flávia de Souza Bastos, Lucas Machado Rocha, Rafael Grande Pancini Delmonte, and Afonso Celso de Castro Lemonge. Evaluation of low fidelity and cfd methods for the aerodynamic performance of a small propeller. *Aerospace Science and Technology*, 108:106402, 2021.

Rajat Mittal and Gianluca Iaccarino. Immersed boundary methods. *Annual Review of Fluid Mechanics*, 37(1):239–261, 2005. doi: 10.1146/annurev.fluid.37.061903.175743.

Charles Samuel Peskin. *Flow patterns around heart valves: a digital computer method for solving the equations of motion*. Yeshiva University, 1972.

William John Macquorn Rankine. On the mechanical principles of the action of propellers. *Transactions of the Institution of Naval Architects*, 6, 1865.

M Ravensbergen, A Bayram Mohamed, and A407294407196712 Korobenko. The actuator line method for wind turbine modelling applied in a variational multiscale framework. *Computers & Fluids*, 201:104465, 2020.

Manelisi Kagame Rwigema. Propeller blade element momentum theory with vortex wake deflection. In *27th International congress of the aeronautical sciences*, volume 1, pages 727–735, 2010.

Jens N Sørensen and Asger Myken. Unsteady actuator disc model for horizontal axis wind turbines. *Journal of Wind Engineering and Industrial Aerodynamics*, 39(1-3):139–149, 1992.

Jens Norkær Sorensen and Wen Zhong Shen. Numerical modeling of wind turbine wakes. *J. Fluids Eng.*, 124(2):393–399, 2002.

PR Spalart and SR Allmaras. A one-equation turbulence model for aerodynamic flows. 1994.

Renato Tognaccini. Dell'ala rotante. 2014.

Fred E Weick. *Full scale wind tunnel tests with a series of propellers of different diameters on a single fuselage*. US Government Printing Office, 1930.

David C Wilcox et al. *Turbulence modeling for CFD*, volume 2. DCW industries La Canada, CA, 1998.

TY Wu et al. Flow through a heavily loaded actuator disc. *Schiffstechnik*, 9(47):134–138, 1962.